*Journal of Naval Sciences and Engineering*
*2022, Vol. 18, No. 2, pp. 205-230*
*Electrical-Electronics Engineering/Elektrik-Elektronik Mühendisliği*

*RESEARCH ARTICLE*

**An ethical committee approval and/or legal/special permission has not been required within the scope of this study.*

# THE EFFECT OF FOV ANGLE ON A RSSI-BASED VISIBLE LIGHT POSITIONING SYSTEM*

**Özlem AKGÜN**

*Barbaros Naval Sciences and Engineering Institute, National Defence University, Istanbul, Turkey,*
*oakgun@dho.edu.tr*

**Received: 24.06.2022** **Accepted: 04.08.2022**

*Özlem AKGÜN*

## ABSTRACT

*The effect of field of view (FOV) angle on the positioning performance in a visible light positioning (VLP) system utilizing light-emitting diodes (LEDs) is examined. Due to its simplicity and low cost, the received signal strength indication (RSSI) technique with trilateration is used for distance measurement. Since being robust to noise sources, the optical code division multiple access (CDMA) is preferred for broadcasting the unique identification and location information of each LED at the same time. LEDs are deployed on the ceiling of a highly reflective room with the aim of providing homogenous and suitable lighting. The varying angle of FOV - $30^o$ up to $88^o$ with $2^o$ increments - is considered in the photodetector (PD) to obtain the effect of FOV on six different VLP scenarios with respect to the number of LEDs. All scenarios have the non-line of sight (NLOS) channel models up to three reflections. Simulation results show that increasing the number of transmitters (Txs) decreases the distance error sensitivity to the changes in the FOV angle. Consequently, indoor scenarios with increased Txs allow the use of low FOV angles. Acceptable distance errors are obtained even in harsh conditions, i.e., near the corner of the room.*

**Keywords:** *Visible Light Positioning, Field of View Angle, Received Signal Strength Indication, Non-Line of Sight Channel Model.*

*The Effect of FOV Angle on a RSSI-based Visible Light Positioning System*

## BİR RSSI TABANLI GÖRÜNÜR IŞIK KONUM BELİRLEME SİSTEMİ ÜZERİNE FOV AÇISININ ETKİSİ


## ÖZ

*Bu çalışmada, ışık yayan diyot (LED) kullanan bir görünür ışık konum belirleme (VLP) sisteminde fotodedektör görüş alanı (FOV) açısının konumlandırma performansı üzerindeki etkisi incelenmiştir. Kolay uygulanabilir ve düşük maliyetli oluşu sebebiyle mesafe ölçümü için trilaterasyon ile birlikte, alınan sinyal şiddeti göstergesi tekniği kullanılmıştır. Her bir LED'in kimlik ve konum bilgisini eş zamanlı yaymak için optik kod bölmeli çoklu erişim tekniği, gürültü kaynaklarına dayanıklı olduğundan tercih edilmiştir. Homojen ve yeterli aydınlatma sağlamak amacıyla LED'ler yüksek yansıtıcılığa sahip bir odanın tavanına yerleştirilmiştir. Görüş açısının etkisini elde etmek üzere altı farklı VLP senaryosunda $30^o$'den $88^o$'ye kadar $2^o$'lik artışlarla fotodedektörün FOV açısındaki değişim dikkate alınmıştır. Her bir senaryo üç yansımaya kadar açık görüş gerektirmeyen kanal modeline sahiptir. Simülasyon sonuçları göstermektedir ki verici sayısını artırmak, FOV açısındaki değişikliklere karşı mesafe hatası duyarlılığını azaltır. Sonuç olarak, artırılmış vericilere sahip iç mekân senaryoları, düşük FOV açılarının kullanılmasına izin verir. Oda köşesi gibi zorlu koşullarda dahi kabul edilebilir mesafe hataları elde edilebilir.*



**Anahtar Kelimeler:** *Görünür Işık Konum Belirleme, Görüş Alanı Açısı, Alınan Sinyal Gücü Göstergesi, Açık Görüş Gerektirmeyen Kanal Modeli.*

## 1. INTRODUCTION

Accurate estimation of a user location is crucial for navigation-based services. In challenging contexts such as indoors, the Global Positioning System (GPS) is inaccurate due to satellites' attenuated and discontinued signals (Zhuang et al., 2018). To overcome this drawback, positioning systems, particularly for indoor environments, utilize indoor wireless signals such as wireless fidelity (Wi-Fi) (Zhuang, Syed et al., 2016), Bluetooth (Hossain & Soh, 2007; Zhuang, Yang et al., 2016), and radio frequency identification (RFID) (Ruiz et al., 2012). These systems, however, have lower positioning accuracy and higher costs (Do & Yoo, 2016; Hassan et al., 2015). Besides, radio frequency (RF) solutions have harmful effects on specific equipment with lower electromagnetic immunity, such as Magnetic Resonance Imaging scanners in health care facilities (Do & Yoo, 2016; Khan, 2017).

The ever-increasing energy demands of the world enable the transition to solid-state lighting (SSL). Energy-efficient LEDs are critical components of this transition. In addition to energy efficiency, LEDs have many key features such as high bandwidth, a long lifetime with reliable lighting, and cost-efficiency. These advantages make LEDs simultaneously used for illumination and indoor positioning (Hann et al., 2010; Lou et al., 2012). Consequently, VLP systems based on LEDs have become extremely popular. Moreover, the VLP system with LEDs obtained more accurate results (0.1-0.35 m positioning error) compared to Wi-Fi (1-7 m), Bluetooth (2-5 m), and RFID (≤2 m) (Hassan et al., 2015).

Major positioning algorithms with trilateration rely on time or signal strength measurement. Such measurements are obtained via the so-called time of arrival (TOA), time difference of arrival (TDOA), and RSSI techniques. TOA, the absolute arrival time of a wireless signal from the Tx to the receiver (Rx), is a powerful technique. However, it requires precisely synchronized Txs and Rxs. An additional timestamp, causing an increase in the complexity, must be added to the transmitting signal (Hui et al., 2007; Zekavat & Buehrer, 2019). TDOA addresses TOA by overcoming the necessity of synchronization between the Txs and the Rxs. But, in TDOA, synchronization is still needed among the Txs to ensure minimum

positioning error (Zhuang et al., 2018). Compared to the techniques mentioned above, the RSSI-based distance measurement using the trilateration algorithm is a promising candidate because of being simple and cost-efficient. Received signal values are easily obtained through a single PD so that there is no need for additional devices. Unlike TOA and TDOA, the performance of RSSI measurements does not strongly depend on the availability of line-of-sight (LOS) channels (Zekavat & Buehrer, 2019). Besides, the trilateration algorithm does not require prior information of an indoor environment as fingerprinting, which is also a positioning algorithm based on the RSSI technique (Guowei et al., 2013; Yiu et al., 2016). Though using the RSSI with trilateration algorithm has attracted much attention, it is generally applied with LOS channels (Kim et al., 2013; Yang et al., 2013; Li et al., 2014; Zhang, Chowdhury et al., 2014). Consequently, research using different channel models, such as those involving NLOS components, is still needed. This study aims to relate the significant advantages of the RSSI-based trilateration positioning algorithm for an NLOS channel model.

The luminous flux emitted from LEDs diffuses in certain directions and reflects from walls, the ceiling, and objects in a room. Though the specular-type light reflections may occur from a shiny object such as a mirror, most reflections are generally diffuse type, which can be modeled well with a Lambertian radiation pattern (Gfeller & Bapst, 1979; Barry, 1994; Kahn et al., 1995). These reflected components of light, briefly NLOS components, significantly contribute to the received signal strength at the PD. In (Mohammed & Elkarim, 2015), the contribution of NLOS components up to three reflections is explored. The localization error distribution for the PD positions in the whole room is obtained for LOS and NLOS cases. In the study (Gu et al., 2016), the effect of multipath reflections on the positioning accuracy is investigated for particularly selected locations. In addition, calibration approaches for selecting LED signals and decreasing the distance between the LEDs are discussed to increase the positioning accuracy. Based on the calibration approach of (Gu et al., 2016), in the work (Tang et al., 2017), the selection of the four strongest LED signals, including multipath reflections, is made by a hybrid algorithm. Then, a weighted centroid algorithm is proposed to detect improved positions. An RSSI-based VLP system with NLOS contributions is studied in (Mousa et al., 2018), where

the system's performance is tested for the case of noisy and noiseless channels. The authors of (Mousa et al., 2018) reported a positioning accuracy of less than 10 cm at a signal-to-noise ratio (SNR) value of more than 12 dB. In the study (Çelik, 2019), with the motivation to increase the overall system performance of RSSI-based VLP, homogeneous illumination is aimed to maximize the individual SNR of each LED. Consequently, the effect of LED deployment is studied to fulfill the aim. Increasing the number of LEDs resulted implicitly in a decreased mean square error (MSE) of distance (Çelik, 2019). Nevertheless, *most* of these studies were conducted under the assumption of a fixed FOV angle of the PD though it is one of the essential features of a VLP system. A switching estimated receiver position scheme is proposed by (Sertthin et al., 2009), where the experiments were performed for three different types of FOV receivers. Each receiver has a constant FOV angle: 25°, 17.5°, and 10°. In the study, however, the distance error performance is analyzed with respect to the tilt angle of a 6-axes geomagnetic and gravity acceleration sensor that increases the complexity of the system. Besides, a two-dimensional positioning error of $29.8\ cm$ was reported for the FOV angle of 10° as the best case. A two-phase hybrid algorithm additional to the conventional triangulation is proposed by (Prince & Little, 2012), where the FOV angle as a function of the receiver's azimuth and elevation orientation is discussed. Course-phase algorithm is tested for FOV angles to detect poor or numerically ill-defined locations. Observations showed that a course estimation could not be made for some orientation configurations when $FOV \notin [70°, 110°]$. The most accurate position estimation is provided for the FOV angle of 90° since the receiver could not detect enough light for a smaller FOV angle to make a positioning estimation. Distributions of received power, SNR, and BER are given by (Sendani & Ghahramani, 2017) for three different FOV angles: 30°, 60°, and 90°. Although the authors did not precisely mention the number of transmitters in the system, according to Figure 1 of the study, only four Txs in a single indoor scenario were considered. Besides, the authors did not discuss the positioning accuracy of the system, which was examined only in the framework of visible light communication (VLC). In the study of (Seguel et al., 2019), FOV analysis is given for imaging receivers to test the proposed algorithm according to the parameter changes of the detector. The authors reported that FOV angles have low impact on

the proposed algorithm, which is an expectable fact since four PDs are used to form an imaging receiver. Additionally, the effect of multipath reflections is not considered in the studies of (Sertthin et al., 2009; Sendani & Ghahramani, 2017; Seguel et al., 2019).

To accurately estimate a position on the PD plane using the trilateration algorithm, at least three LEDs with known locations are required from the LOS model of the channel in the VLP system (Xu et al., 2017). Therefore, NLOS contributions in the RSSIs degrade the localization performance of the VLP. Choosing a small FOV angle in the PD seems to be an easy solution to minimize these contributions. However, it is not too realistic for an indoor environment. Since the vertical distance between the PD plane and the ceiling is constant, the minimum FOV angle of the PD depends on the distances between the Tx points. These distances vary according to the number of Txs used in the indoor scenario, so does FOV. This fact is the primary motivation of our study as we investigate the effect of FOV angle via considering various numbers of indoor scenarios on the performance of RSSI-based VLP system.

## 2. SYSTEM OVERVIEW

We consider a generalized indoor environment of cubic space, which we will refer to as a room for the rest of the study. Figure 1 illustrates a typical prototype of the system model, where several Txs are deployed on the ceiling for illumination. We assume that the Txs are 0.5 m below the ceiling plane, and a PD is placed anywhere in the room at 0.85 m in height above the ground plane. These assumptions are the same as in the studies (Mohammed & Elkarim, 2015; Çelik, 2019). Each Tx in Figure 1 transmits a unique global identification (ID) code in addition to its local coordinates with respect to the room's origin. The major challenge in the VLP system is to determine the PD's local position from Txs' location coordinates. Once the PD's position is determined, the PD may send its local position to a server. The origin of the room in the local coordinate has a known latitude, longitude, and altitude in the global coordinate. Thus, the server transforms the PD position into a global coordinate.

Each Tx in the room needs a processor for encoding global IDs and local coordinates into bit sequences. Then, a driver circuit switches the LEDs in a

Tx into an on-off state based on a particular modulation scheme. A frequently used method for modulation is the On-Off Keying (OOK). Bit sequences modulate the intensity of the light emitted from each LED. That is why the technique is called intensity modulation (IM). Since there are multiple Txs in the room, a multiplexing protocol is required to distinguish the different signals of each Tx. In this study, as the multiplexing technique, we use the optical CDMA (Lausnay et al., 2015; Lausnay et al., 2014), which can easily be implemented by the OOK modulation and the Walsh codes. Unlike RF communication systems employing complex-valued bipolar signals, VLC (Celik & Çolak, 2020) systems require unipolar real-valued signals when modulating light. A DC bias signal and a turn-off-voltage are added to the bipolar CDMA signal to obtain a unipolar one at the Tx side. The resulting electrical signal is used by the driver circuit switching the LEDs. At the Rx side, we consider the direct detection of the optical carrier belonging to the incoherent light source simply the LEDs. Thus, the baseband VLC channel model, used in this study, is given by (Kahn et al., 1995; Komine et al., 2009; Zhou et al., 2012)

$$y(t) = x(t) \otimes h(t) + n(t), \tag{1}$$

where $y(t)$ is the output photocurrent, $x(t)$ is the non-negative optical input power, $h(t)$ is the channel's impulse response, and the symbol "$\otimes$" stands for the convolution. In Eq.(1), $n(t)$ corresponds to the signal-independent additive Gaussian noise. There are two types of noise mainly affecting the PD current. One is the shot noise caused by the incident optical power, which includes the desired signal and the background light already present in the VLP environment. Although the background light components in the Rx can be reduced by optical filtering, it still causes shot noise. The second is the thermal noise due to the increasing temperature of the PD during its working process. Thus, in this study, we model the noise, $n(t)$, as a signal-independent, zero-mean Gaussian random variable whose variance is $\sigma^2 = N_0/2$ per dimension. The time-average transmitted optical power which is emitted from each LED in the $i^{th}$ Tx can be written as

$$P_{t,i}^{o} = \frac{1}{T_c} \int_0^{T_c} x_i(t)\, dt, \tag{2}$$

where $T_c$ is the chip period of the optical CDMA signal. When the optical CDMA signal reaches Rx, the DC component of the photocurrent is first filtered out so that the orthogonality between the CDMA codes is preserved. Next, correlation with known code sequences is performed. After decoding the CDMA signal, the received signal strength is measured and sent as input to the positioning estimator.

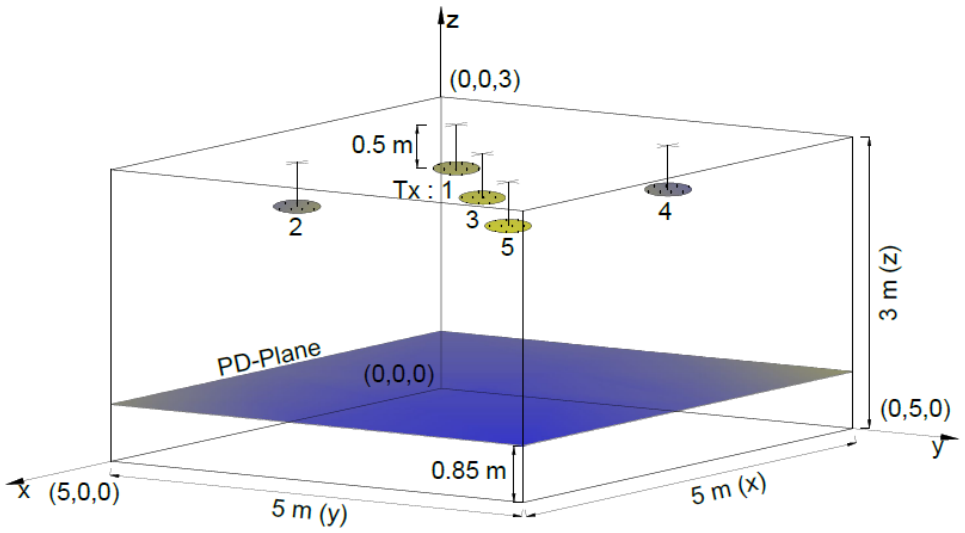


**Figure 1.** Indoor geometry for $N_t = 5$.

In this study, we have adopted six different VLP scenarios from (Çelik, 2019) with respect to the number of Txs, $N_t$, to examine the FOV effect which is not discussed in (Çelik, 2019). In each scenario, it is assumed that transmitters are deployed on the ceiling, thereby obtaining the maximum individual SNR from each Tx. The deployment of $N_t$ transmitters also ensures illumination with a non-flicking effect. These are strong reasons to adopt the indoor scenarios of the study (Çelik, 2019). The coordinates for varying number of Txs are given in Table 1. According to (Qiu et al., 2018), the VLC-CDMA system using OOK has an SNR value of 20 dB when the bit error ratio (BER) almost reaches $10^{-3}$ for bipolar-to-unipolar codes with 16 users. As stated by (Qiu et al., 2018), these results are sufficient enough to acquire reliable VLC with CDMA based OOK modulation. Since the study (Çelik, 2019) reported a minimum SNR value of 45 dB for its VLP

scenarios, and this value is much better than the one in (Qiu et al., 2018), we conclude that the multiple access interference (MAI) is prevented thoroughly in our study.

**Table 1.** x-y positions of Txs.

| $N_t$ | **x-y positions (m)** |
|---|---|
| **4** | {1.25-1.25; 1.25-3.75; 3.75-1.25; 3.75-3.75} |
| **5** | {1.03-1.03; 3.96-1.03; 2.50-2.50; 1.03-3.96; 3.96-3.96} |
| **8** | {0.85-0.85; 4.14-0.85; 2.50-1.29; 1.29-2.50; 3.70-2.50; 2.50-3.70; 0.85-4.14; 4.14-4.14} |
| **9** | {0.83-0.83; 2.50-0.83; 4.16-0.83; 0.83-2.50; 2.50-2.50; 4.16-2.50; 0.83-4.16; 2.50-4.16; 4.16-4.16} |
| **12** | {0.70-0.70; 3.10-0.70; 1.90-1.46; 4.29-1.46; 0.70-2.12; 3.10-2.12; 1.90-2.87; 4.29-2.87; 0.70-3.54; 3.10-3.54; 1.90-4.29; 4.29-4.29} |
| **16** | {0.62-0.62; 1.87-0.62; 3.12-0.62; 4.37-0.62; 0.62-1.87; 1.87-1.87; 3.12-1.87; 4.37-1.87; 0.62-3.12; 1.87-3.12; 3.12-3.12; 4.37-3.12; 0.62-4.37; 1.87-4.37; 3.12-4.37; 4.37-4.37} |

## 3. METHODOLOGY

### 3.1. Optical Received Power

In the channel model, we consider the LOS and the NLOS link with three reflections for varying numbers of Txs, particularly, $N_t$ = 4, 5, 8, 9, 12, and 16. The relating channel gain coefficient for the VLC link between the $i^{th}$ Tx and the single Rx is given by $h_i$, having two components as follows

$$h_i = h_i^{LOS} + \sum_{n=1}^{k} h_i^{NLOS(n)}, \tag{3}$$

where $n$ counts the number of reflections; $n = \{1, 2, \dots, k\}$, particularly, $k = 3$ as we consider three reflections. Since a Lambertian pattern of radiation models the diffuse-type reflections well, $h_i^{LOS}$ is written by (Barry, 1994)

$$h_i^{LOS} = \frac{(m+1)A}{2\pi d_i^2}\cos^m(\alpha_i)\cos(\beta_i)\,\mathrm{rect}\left(\frac{\beta_i}{FOV}\right), \tag{4}$$

where $m$ represents the order of the Lambertian radiation pattern and is related to the semi-angle at half illuminance of the LED. $A$ is the PD's effective area. The link distance between the $i^{th}$ Tx and the PD is given by $d_i$. While the argument $\alpha_i$ measures the angle of emergence from the Tx's plane normal to the link between the $i^{th}$ Tx and the PD, $\beta_i$ measures the angle of incidence from the PD's plane normal. Since the ceiling and the PD planes are parallel, $\alpha_i$ is equal to $\beta_i$ for the LOS link. The $FOV$ denotes the PD's field of view angle. Finally, the rectangular function, $\mathrm{rect}\left(\frac{\beta_i}{FOV}\right)$, equals 1 when the absolute value of its argument is lesser or equal to 1, otherwise it is 0.

As noted in the previous section, most reflections of the visible light rays are generally of the diffuse type as room surfaces are rough compared to the wavelength of visible light. Therefore, it is assumed that the room surfaces consist of numerous differential areas, each of which acts as a transmitter that emits light rays independent of the angle of incidence. Each differential transmitter has a Lambertian radiation pattern then, the NLOS channel gain coefficient from the $i^{th}$ Tx with $k$ reflections is as follows (Lee et al., 2011)

$$h_i^{NLOS(k)} = L_i^{(1)}L_i^{(2)} \ldots L_i^{(k+1)}\,\mathrm{rect}\left(\frac{\beta_i^{(k+1)}}{FOV}\right), \tag{5}$$

where

$$\begin{aligned} L_i^{(1)} &= \frac{(m+1)dA}{2\pi d_{i(1)}^2}\cos^m\left(\alpha_i^{(1)}\right)\cos\left(\beta_i^{(1)}\right), \\ L_i^{(2)} &= \frac{dA}{\pi d_{i(2)}^2}\cos^m\left(\alpha_i^{(2)}\right)\cos\left(\beta_i^{(2)}\right)\rho_i^{(2)}, \\ L_i^{(k+1)} &= \frac{dA}{\pi d_{i(k+1)}^2}\cos^m\left(\alpha_i^{(k+1)}\right)\cos\left(\beta_i^{(k+1)}\right)\rho_i^{(k+1)}. \end{aligned} \tag{6}$$

In Eq.(6), $dA$ is the differential area of the reflecting surface. The parameter $d_{i(1)}$ represents the link distance between the $i^{th}$ Tx and the first differential surface, whereas $d_{i(k+1)}$ denotes the distance after the $k^{th}$ reflection to the PD. The argument $\alpha_i^{(1)}$ measures the angle of emergence from the $i^{th}$ Tx plane normal to the link up to the first differential surface. Similarly, $\beta_i^{(1)}$ measures the angle of incidence to the first differential reflecting surface. The arguments $\alpha_i^{(k+1)}$ and $\beta_i^{(k+1)}$ represent the emergence and the incidence angles after the $k^{th}$ reflections from the $i^{th}$ Tx, respectively. The parameter $\rho_i^{(k+1)}$ is the reflection coefficient indicating the proportion of diffusive reflection of the $k^{th}$ reflecting surface (Gfeller & Bapst, 1979).

In a multipath channel, the power delay profile (PDP) represents the intensity of the received signal as a function of time delay. According to the PDP analysis, if the correlation bandwidth of the channel is much larger than the bandwidth of the signal, inter-symbol interference (ISI) is not an issue through the channel. In (Çelik, 2019), the PDP analysis of the channel is examined for some of the indoor scenarios adopted in our study. The analysis showed that the ISI effect could be completely ignored for the indoor scenarios under study. In other words, the intensity of light emitted from Txs in a symbol period is received within the same period. Hence, the optical channel consists of the light intensity collected in a symbol period regardless of time. This fact is another strong reason for adopting the channel models in the study (Çelik, 2019). Therefore, without loss of significance, we may assume that the optical filter gain, $T_s(\beta)$, and the optical concentrator gain, $G(\beta)$, are equal to 1. Finally, the optical received power can be written as follows (Komine et al., 2009)

$$P_r^o = \sum_{i=1}^{N_t} P_i^o \, h_i, \tag{7}$$

where $P_i^o$ is the optical power emitted from each LED in the $i^{th}$ Tx and equals $0.45\sqrt{W}$. To ensure a fair comparison between the indoor scenarios with respect to the number of Txs, $N_t$, we keep the total optical power constant, which is $P_{tot}^o = 324\sqrt{W}$, by arranging different numbers of LEDs

in each indoor scenario. Table 2 shows the number of LEDs, $N_{LED}$, contained in the Txs, and the optical power of each Tx, $P_{Tx}^{o}$.

**Table 2.** Tx Parameters.

| $N_t$ | $N_{LED}$ | $P_i^o\ (\sqrt{W})$ | $P_{Tx}^o\ (\sqrt{W})$ | $P_{tot}^o\ (\sqrt{W})$ |
|---|---|---|---|---|
| *4* | *180* | *0.45* | *81* | *324* |
| *5* | *144* | | *64.8* | |
| *8* | *90* | | *40.5* | |
| *9* | *80* | | *36* | |
| *12* | *60* | | *27* | |
| *16* | *45* | | *20.25* | |

### 3.2. RSSI-Based Trilateration Algorithm

This subsection examines the trilateration positioning algorithm based on the RSSI technique. Once the PD has received the transmitted data, the signals from different Txs are separated through the CDMA decoder thanks to the orthogonality of the codes. The PD determines the locations of the Txs, and also measures the electrical power of the received signal from each Tx. The trilateration algorithm (Gu et al., 2014) generally uses at least four link distances between the Txs and the PD to determine the exact location of the PD in three-dimensional (3D) space. Since the link and the vertical distances are not available for an unknown PD location, an iteration algorithm is applied to provide the 3D coordinates of the PD. By estimating the height of the PD to the final estimation, the link distance is calculated, from which the horizontal distance between the Txs and the PD is determined. If the PD is mobile in a known plane, see Figure 1, then, three Txs with known location data are sufficient for the algorithm to adequately determine the PD's position.

A PD which is a direct-detection (DD) receiver has the square-law nature (Barry, 1994). This means that its output electric power is proportional to the square of the input optical power. Hence, the electrical power received from the $i^{th}$ Tx is written as follows

$$P_{r(i)}^{\mathrm{e}} = (P_i^o h_i R)^2, \tag{8}$$

where $R$ is the responsivity of the PD. For the LOS link, the angles $\alpha_i$ and $\beta_i$ in Eq.(4) are equal to each other so we can write the following relation

$$cos^{(m+1)}(\alpha_i) = \left(\frac{d_v}{d_i}\right)^{(m+1)} \tag{9}$$

in terms of the link distance, $d_i$, and the vertical distance between the Tx and the PD planes, where $d_v = 1.65\ m$. After substituting Eq.(9) and Eq.(4) into Eq.(8), we get the link distance between the $i^{th}$ Tx and the PD as follows

$$d_i = \sqrt[(2m+6)]{\frac{\left(RP_i^o(m+1)A\, d_v^{(m+1)}\right)^2}{4\pi^2 P_{r(i)}^{\mathrm{e}}}}. \tag{10}$$

Once the link distance is calculated via Eq.(10), at least three horizontal distances between the $i^{th}$ Tx and the PD can easily be determined. These horizontal distances can be expressed as (Gu et al., 2014)

$$\begin{aligned} d_1^2 &= (x_{Rx} - x_1)^2 + (y_{Rx} - y_1)^2 + (z_{Rx} - z_1)^2, \\ d_2^2 &= (x_{Rx} - x_2)^2 + (y_{Rx} - y_2)^2 + (z_{Rx} - z_2)^2, \\ d_3^2 &= (x_{Rx} - x_3)^2 + (y_{Rx} - y_3)^2 + (z_{Rx} - z_3)^2. \end{aligned} \tag{11}$$

Here, $(x_{Rx}, y_{Rx}, z_{Rx})$ is the coordinates of the PD in 3D space, whereas the other coordinates at the right-hand sides of Eq.(11) belong to the three Txs. The last terms for the $z$ −coordinates of Eq. (11) are all the same since the PD is mobile in the plane with a known altitude. Therefore, subtracting the second and the third equations from the first of Eq.(11) yields the following matrix (Kim et al., 2013)

$$\mathbf{B} = \mathbf{A}\mathbf{x}, \tag{12}$$

where

$$\begin{aligned} \mathbf{B} &= \frac{1}{2}\begin{bmatrix} d_1^2 - d_2^2 + x_2^2 + y_2^2 - x_1^2 - y_1^2 \\ d_1^2 - d_3^2 + x_3^2 + y_3^2 - x_1^2 - y_1^2 \end{bmatrix}, \\ \mathbf{A} &= \begin{bmatrix} x_2 - x_1 & y_2 - y_1 \\ x_3 - x_1 & y_3 - y_1 \end{bmatrix}, \quad \mathbf{x} = \begin{bmatrix} x_{Rx} \\ y_{Rx} \end{bmatrix}. \end{aligned} \tag{13}$$

Eq.(12) can be solved using the linear least square method that is $\mathbf{x} = (\mathbf{A}^{\mathrm{T}}\mathbf{A})^{-1}\mathbf{A}^{T}\mathbf{B}$ (Reichenbach et al., 2006).

The received signal strength is sensitive to the indoor environment; therefore, neglecting noise in a VLP system has unrealistic consequences that should be avoided. As stated in the previous section, we model the noise parameter as the signal-independent additive Gaussian noise with a variance of $\sigma^2$. The variance is equal to the noise power as its mean value is zero. In (Çelik, 2019), the noise power of the system model is calculated as $2.5 \times 10^{-12}\ W$ by using the noise parameters of (Zhang, Duan et al., 2014). Another essential parameter for determining the performance of a VLP system is the signal-to-noise ratio (SNR). The electrical SNR for the $i^{th}$ Tx in terms of $\sigma^2$ is given as follows

$$SNR_i = \frac{P^{\mathrm{e}}_{r(i)}}{\sigma^2}. \tag{14}$$

According to (Mohammed & Elkarim, 2015), in the case of the LOS link, the highest received signal power is obtained just under the Txs, where *only* $N_t = 4$ is studied whose locations are the same as ours, see Table 1. The main factor controlling the localization accuracy is the SNR since the minimum localization error, $0.18\,mm$, is obtained where the best SNR value is recorded. As the Rx moves to the room corners, the received power gradually decreases. The minimum SNR value is obtained at the corner; consequently, the worst localization error is recorded as $14.06\,cm$. For the overall link, which consists of LOS and NLOS components, a dramatic increase in the received power near the walls is observed due to their high reflectivity. The reflections have a minor effect at the room center; hence, the SNR is at its maximum value, whereas the localization error is minimal, $6\,cm$. However, the latter localization error is far worse than that of the LOS link. From this fact, we can conclude that although we have to consider the NLOS contribution for a realistic model of a VLP system, the contribution must be reduced. In this study, the following section with *novel* results discusses the role of $FOV$ in reducing the negative effect of NLOS contribution on the positioning accuracy.

## 4. SIMULATIONS

This section presents the simulation results for the distance error performance with respect to the $FOV$ angle. Table 3 summarizes the simulation parameters for the considered VLP system.

**Table 3.** Simulation parameters.

| | |
|---|---|
| Elevation of the LEDs | -90º |
| Azimuth of the LEDs | 0º |
| Semi-angle at half power $(\Phi_{1/2})$ | 60º |
| Lambertian order $(m)$ | 1 |
| Elevation of the PD | 90º |
| Azimuth of the PD | 0º |
| Responsivity $(R)$ | 0.4 $A/\sqrt{W}$ |
| Area of the PD $(A)$ | 0.0001 $m^2$ |
| Wall reflectivity coefficient $(\rho_w)$ | 0.8 |
| Ceiling reflectivity coefficient $(\rho_c)$ | 0.5 |
| Floor reflectivity coefficient $(\rho_f)$ | 0.3 |
| Area of differential elements $(dA)$ | 0.04 $m^2$ |

In the simulations, we select three typical PD positions to analyze the effect of the $FOV$ angle on the distance error performance of the VLP system. The first location is near the center of the room, the other is near the wall edge, and the third location is near the corner of the room, which is the severest case considering the multipath reflections. Figure 2 shows the distance error versus the *FOV* angle when the PD is located near the center of the room. It can be seen from Figure 2 that for the indoor scenario with $N_t = 12$, the best performance is obtained for the *FOV* angles from 32º up to 88º. If a generalization is made from the figure, we can say that the distance error performance improves with the increasing number of Txs, so that the sensitivity of the distance error to the $FOV$ angle decreases. The exceptions to this generalization are the indoor scenarios for $N_t = 5$, and 9 due to the LED deployment that takes into account the illumination issues, see (Çelik,

2019). For those cases, the distance error increases significantly due to the increase in the $FOV$ angle. Another important extraction from Figure 2 is that an increase in the number of Txs allows lower $FOV$ angles since at least three Txs must be in the range of the PD due to the trilateration algorithm. This fact also results in reduced reflected signals and improved distance error performance.

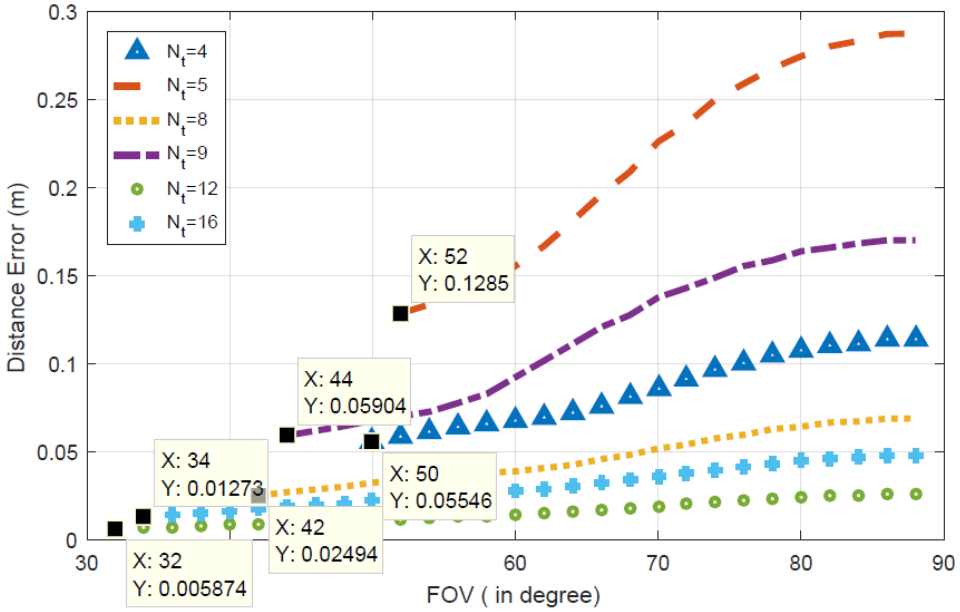


**Figure 2.** Distance error with respect to the $FOV$ angle for the PD position near the center of the room.

Figure 3 demonstrates the distance error performance when the PD is near the left wall edge, chosen intentionally to take severe reflections from one wall. For the left wall, we refer to a typical room geometry in which the left wall is between the wall with an entrance to the room and the wall having windows. The indoor scenarios for $N_t = 5$, 12, and 16 achieve the minimum distance error with low sensitivity to the changes in the $FOV$ angle. The general idea that the distance error performance increases with the increasing number of Txs, extracted from Figure 2, is also valid for Figure 3 except for $N_t = 5$. For this case, with the aim of uniform illumination, Tx: 3, located at the center of the ceiling plane, pushes the

illuminance of the other four toward the corners, see Figure 1. Thus, the reflections going through the PD weaken for this indoor scenario. Another remarkable situation is that the distance error sensitivity to the $FOV$ angle is very high for $N_t = 8$. When we compare the ordinates of Figure 2 and Figure 3, the distance error gets worse for Figure 3 due to the PD location near the wall edge, which causes severe reflections.

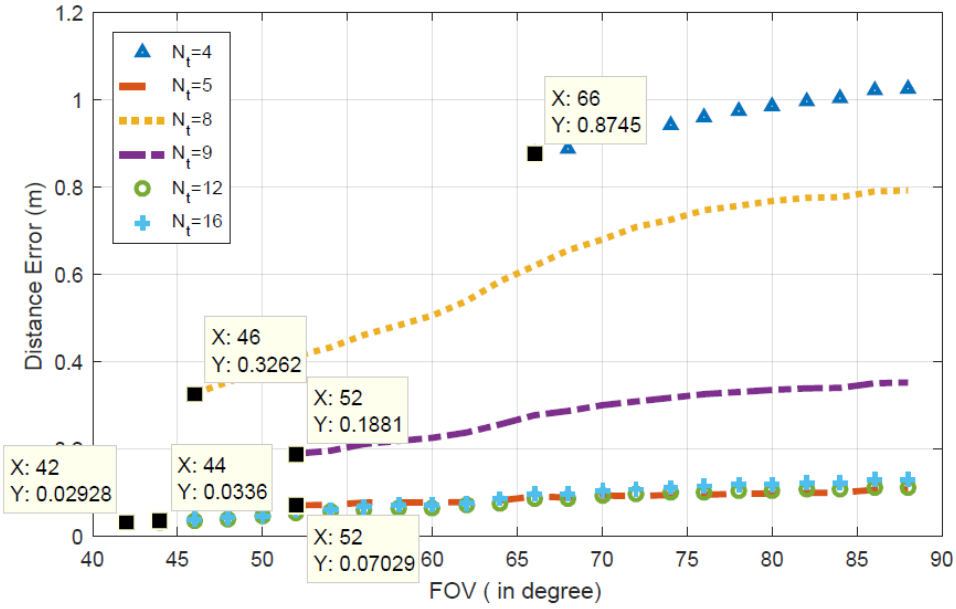


**Figure 3.** Distance error with respect to the $FOV$ angle for the PD position near the left wall of the room.

In Figure 4, we show the distance error versus the $FOV$ angle for the PD location near the corner of the room, chosen as the severest case due to intense reflections from the four walls. Compared to others, the scenarios with $N_t = 12$ and 16 achieve minimum distance errors for all *available* $FOV$ angles. Besides, the distance error sensitivity to the $FOV$ angle increases noticeably for these cases. As expected, when we compare the ordinates of Figures 2, 3, and 4, the distance error is the worst for Figure 4. However, it is still possible to achieve satisfactory error performances, i.e., $0.049\ m$, using an increased number of Txs and low $FOV$ angles, i.e., $40^{\circ}$.

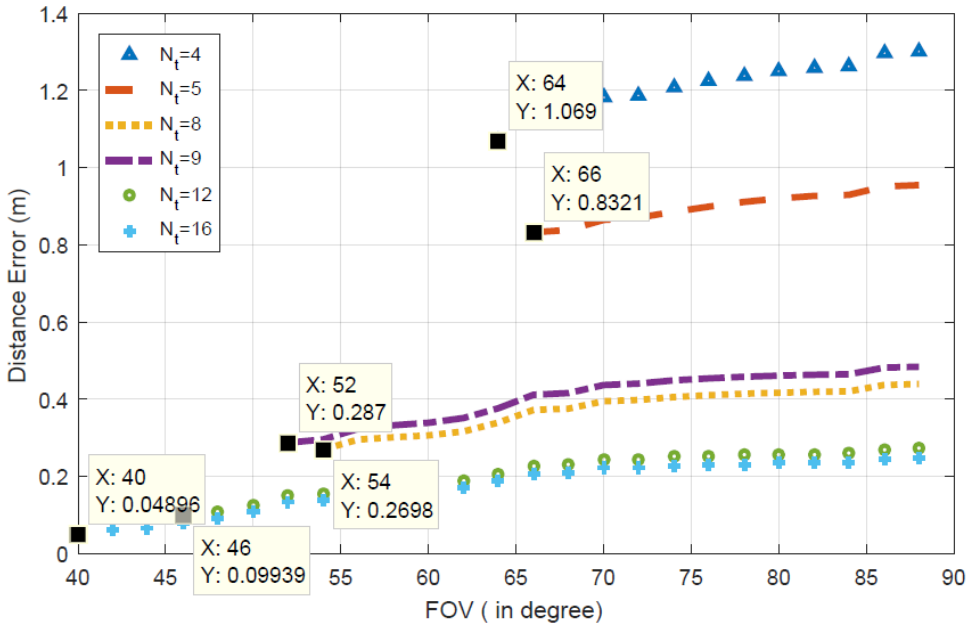


**Figure 4.** Distance error with respect to FOV in the position close to the corner of the room for different indoor scenarios.

## 5. CONCLUSION

In this study, we have investigated the effect of the $FOV$ angle of a planar PD for an RSSI-based VLP system. We have also considered illumination constraints in the system model. Positioning errors are evaluated according to the number of Txs, particularly $N_t = 4, 5, 8, 9, 12$, and 16 at varying $FOV$ angles from $30^{\circ}$ to $88^{\circ}$ with $2^{\circ}$ increments. Simulation results have demonstrated that increasing the number of Txs decreases the distance error sensitivity to the changes in the $FOV$ angle. Consequently, indoor scenarios with increased transmitters allow the use of low $FOV$ angles. Besides, acceptable distance errors are obtained even in harsh conditions, i.e., near the corner of the room.

**CONFLICT OF INTEREST STATEMENT**

The author declares no conflict of interest.

## REFERENCES

Barry, J. R. (1994). *Wireless Infrared Communications*. New York: Springer.

Celik, Y., & Çolak, S. A. (2020). "Quadrature spatial modulation sub-carrier intensity modulation (QSM-SIM) for VLC". *Physical Communication, 38*, 1-10.

Çelik, Y. (2019). "The effect of LED deployment on RSSI-based VLP systems". *European Journal of Science and Technology, 17*, 823-832.

Do, T. H., & Yoo, M. (2016). "An in-depth survey of visible light communication based positioning systems". *Sensors, 16*(5), 1–40.

Gfeller, F. R., & Bapst, U. (1979). "Wireless in-house data communication via diffuse infrared radiation". *Proceedings of the IEEE, 67*(11), 1474–1486.

Gu, W., Aminikashani, M., Deng, P., & Kavehrad, M. (2016). "Impact of multipath reflections on the performance of indoor visible light positioning systems". *Journal of Lightwave Technology, 34*(10), 2578–2587.

Gu W., Zhang, W., Kavehrad, M., & Feng, L. (2014). "Three-dimensional light positioning algorithm with filtering techniques for indoor environments". *Optical Engineering, 53*(10), 107107-1–107107-11.

Guowei, Z., Zhan, X., & Dan, L. (2013). "Research and improvement on indoor localization based on RSSI fingerprint database and K-nearest neighbor points". *International Conference on Communications, Circuits and Systems* (pp. 68-71). Chengdu, China.

Hann, S., Kim, J. H., Jung, S. Y., & Park, C. S. (2010). "White LED ceiling lights positioning systems for optical wireless indoor applications". *36th European Conference and Exhibition on Optical Communication* (pp. 1–3). Torino, Italy.

Hassan, N. U., Naeem, A., Pasha, M. A., Jadoon, T., & Yuen, C. (2015). "Indoor positioning using visible LED lights: A survey". *ACM Computing Surveys, 48*(2), 1–32.

Hossain, A. K. M. M. & Soh, W. S. (2007). "A comprehensive study of Bluetooth signal parameters for localization". *18th IEEE Annual International Symposium on Personal, Indoor and Mobile Radio Communications* (pp. 1–5). Athens, Greece.

Hui, L., Darabi, H., Banerjee, P., & Liu, J. (2007). "Survey of wireless indoor positioning techniques and systems". *IEEE Transactions on Systems, Man and Cybernetics-Part C: Applications and Reviews, 37*(1), 1067–1080.

Kahn, J. M., Krause, W. J., & Carruthers, J. B. (1995). "Experimental characterization of non-directed indoor infrared channels". *IEEE Transactions on Communications, 43*(2/3/4), 1613–1623.

Khan, L. U. (2017). "Visible light communication: Applications, architecture, standardization and research challenges". *Digital Communications and Networks, 3*(2), 78–88.

Kim, H. S., Kim, D. R., Yang, S. H., Son, Y. H., & Han, S. K. (2013). "An indoor visible light communication positioning system using a RF carrier allocation technique". *Journal of Lightwave Technology, 31*(1), 134–144.

Komine, T., Lee, J. H., Shinichiro, H., & Nakagawa, M. (2009). "Adaptive equalization system for visible light wireless communication utilizing multiple white LED lighting equipment". *IEEE Transactions on Wireless Communications, 8*(6), 2892-2900.

Lausnay, S. D. Strycker, L. D., Goemaere, J. P., Stevens, N., & Nauwelaers, B. (2014). "Optical CDMA codes for an indoor localization system using VLC". *3rd International Workshop in Optical Wireless Communications* (pp. 1-5). Funchal, Madeira, Portugal.

Lausnay, S. D. Strycker, L. D., Goemaere, J. P., Stevens, N., & Nauwelaers, B. (2015). "Influence of MAI in a CDMA VLP system". *International Conference on Indoor Positioning and Indoor Navigation* (pp. 1–9). Banff, AB, Canada.

Lee, K., Park, H., & Barry, J. R. (2011). "Indoor channel characteristics for visible light communications". *IEEE Communications Letters, 15*(2), 217–219.

Li, L., Hu, P., Peng, C., Shen, G., & Zhao, F. (2014). "Epsilon: A visible light based positioning system". *11th USENIX Symposium Networked Systems Design and Implementation* (pp. 331–343). Seattle, WA, USA.

Lou, P., Zhang, H., Zhang, X., Yao, M., & Xu, Z. (2012). "Fundamental analysis for indoor visible light positioning system", *1st International Workshop on Optical Wireless Communications* (pp. 59–63). Bejing, China.

Mohammed, N. A., & Elkarim, M. A. (2015). "Exploring the effect of diffuse reflection on indoor localization systems based on RSSI-VLC". *Optics Express, 23*(16), 20297–20313.

Mousa, F. I. K., Almaadeed, N., Busawon, K., Bouridane, A., Binns, R., Elliot, I. (2018). "Indoor visible light communication localization system utilizing received signal strength indication technique and trilateration method". *Optical Engineering, 57*(1), 1–10.

Prince, G. B., & Little, T. D. C. (2012). "A two phase hybrid RSS/AoA algorithm for indoor device localization using visible light". IEEE Global Communications Conference (pp. 3347-3352). Anaheim, CA, USA.

Qiu, Y., Chen, S., Chen, H. H., & Meng, W. (2018). "Visible light communications based on CDMA technology". *IEEE Wireless Communications, 25*(2), 178–185.

Reichenbach F., Born, A., Timmermann, D., & Bill, R. (2006). "A distributed linear least squares method for precise localization with low complexity in wireless sensor networks". *2nd IEEE International Conference on Distributed Computing in Sensor Systems* (pp. 514-528). San Francisco, CA, USA.

Ruiz, A. R. J., Granja, F. S., Honorato, J. C. P., & Rosas, J. I. G. (2012). "Accurate pedestrian indoor navigation by tightly coupling foot-mounted IMU and RFID measurements". *IEEE Transactions on Instrumentation and Measurement, 61*(1), 178–189.

Seguel, F., Krommenacker, N., Charpentier, P., & Soto, I. (2019). "A novel range free visible light positioning algorithm for imaging receivers".*Optik, 195*, 163028-1–163028-21.

Sendani, N., & Ghahramani, R. (2017). "Study the effect of FOV in Visible Light Communication". *International Research Journal of Engineering and Technology, 4*(10), 759-763.

Sertthin, C., Tsuji, E., Nakagawa, M., Kuwano, S., & Watanabe, K. (2009). "A switching estimated receiver position scheme for visible light based indoor positioning system," *4th International Symposium on Wireless Pervasive Computing* (pp. 1–5). Melbourne, Australia.

Tang, W., Zhang, J., Chen, B., Liu, Y., Zuo, Y., Liu, S., Dai, Y. (2017). "Analysis of indoor VLC positioning system with multiple reflections". *16th International Conference on Optical Communications and Networks* (pp. 1–3). Wuzhen, China.

Xu, Y., Wang, Z., Liu, P., Chen, J., Han, S., … Yu, J., (2017). "Accuracy analysis and improvement of visible light positioning based on VLC system using orthogonal frequency division multiple access". *Optics Express, 25*(26), 32618–32630.

Yang, S. H., Jeong, E. M., Kim, D. R., Kim, H. S., Son, Y. H., Han, S. K. (2013). “Indoor three-dimensional location estimation based on LED visible light communication”. *Electronics Letters, 49*(1), 1–2.

Yiu, S., Dashti, M., Claussen, H., & Perez-Cruz, F. (2016). “Locating user equipments and access points using RSSI fingerprints: A Gaussian process approach”. *IEEE International Conference on Communications*. (pp. 1-6). Kuala Lumpur, Malaysia.

Zekavat, S. A. R., & Buehrer, R. M. (2019). *Handbook of Position Location: Theory, Practice, and Advances*. Hoboken, NJ: John Wiley & Sons.

Zhang, W., Chowdhury, M. I. S., & Kavehrad, M. (2014). “Asynchronous indoor positioning system based on visible light communications”. *Optical Engineering, 53*(4), 045105-1–045105-10.

Zhang X., Duan, J., Fu, Y., & Shi, A. (2014). “Theoretical accuracy analysis of indoor visible light communication positioning system based on received signal strength indicator”. *Journal of Light Wave Technology, 32*(21), 4180–4186.

Zhou, Z., Kavehrad, M., & Deng, P. (2012). “Indoor positioning algorithm using light-emitting diode visible light communications”. *Optical Engineering, 51*(8), 085009-1–085009-6.

Zhuang, Y., Hua, L., Qi, L., Yang, J., Cao P., Cao Y., … Haas, H. (2018). “A survey of positioning systems using visible LED lights”. *IEEE Communications Surveys & Tutorials*, *20*(3), 1963–1988.

Zhuang, Y., Syed, Z., Li, Y., & El-Sheimy, N. (2016). “Evaluation of two WiFi positioning systems based on autonomous crowdsourcing of handheld devices for indoor navigation”. *IEEE Transactions on Mobile Computing, 15*(8), 1982–1995.

Zhuang, Y., Yang, J., Li, Y., Qi, L., & El-Sheimy, N. (2016). “Smartphone-based indoor localization with Bluetooth low energy beacons”. *Sensors*, *16*(5), 1-20.